Journal of Mines, Metals and Fuels, *73(8): 2405-2413; 2025. DOI: 10.18311/jmmf/2025/49412*

Print ISSN : 0022-2755

Journal of Mines, Metals and Fuels

Contents available at: *www.informaticsjournals.co.in/index.php/jmmf*

Design and Analysis of the Differential Bar of A Rover

Adithya Pillai, Chinmay Dalal, Sakshi Basrur, Hari Vasudevan, Vinayak H. Khatawate* and Pavan Rayar

SVKM's Dwarkadas J. Sanghvi College of Engineering, Vile Parle, Mumbai - 400056, Maharashtra, India; vinayak.khatawate@djsce.ac.in

Abstract

In this paper, the analysis of the differential bar has been performed for the rocker bogie mechanism-based rover to improve the manoeuvrability and its overall stability. The purpose of this differential bar was to increase the stability on rough terrains, increase traction by maximising the grip and avoid wheel slippage. The analysis was performed by considering five materials for the differential bar, viz., aluminium 6061 T6, aluminium alloy, Ti-6Al-4V titanium alloy, Stainless steel 316 annealed and carbon fibre. Solid modelling software was used to design the 3D CAD model of the differential bar, and finite element analysis was performed to optimise the performance of the differential bar. It was found that Ti-6Al-4V titanium alloy was a suitable material for the rover.

Major Findings: *Ti-6Al-4V titanium alloy can be used as an ideal material for differential bars in planetary rovers which operate under extreme environmental conditions.*

Keywords: *Equivalent Strain, Factor of Safety, Finite Element Analysis (FEA), Total Deformation, Wheel Load, Von-Mises Stress*

Abbreviations

FEA	Finite Element Analysis
W	Weight of the rover
L_r	Length of the rocker arm
L_b	Length of the bogie arm
D	Distance from the centre of the rover to each wheel
F	Wheel load or Normal reaction force acting on the wheel
M_r	Moment on the rocker arm
F_d	Force acting on the differential bar
Ti	Titanium
Al	Aluminium
V	Vanadium

1.0 Introduction

The rocker-bogie suspension system of the rover (Figure 1) is capable of extra-terrestrial traversal[1]. The suspension system is the connection of the rover body to the wheels[2]. Even in the absence of stub axles or springs, the rover can overcome obstacles twice the wheel diameter while maintaining the ground contact at all times[3]. A spring absorbs shock while traversing the terrain, but if a differential bar is considered, it distributes and balances the load between the wheels by keeping all the wheels in contact with the ground while overcoming the obstacle. The differential bar is a component which connects the right and left rockers in a

*Author for correspondence

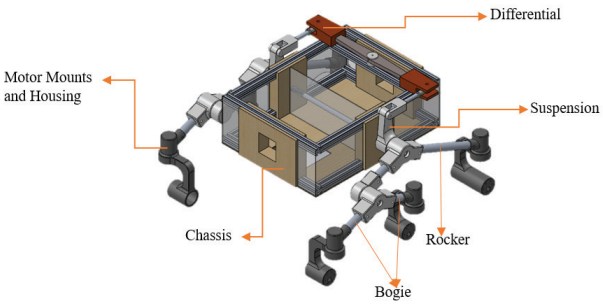


Figure 1. Differential assembly on a rover.

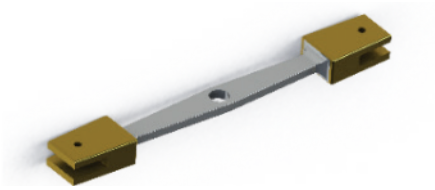


Figure 2. Differential bar.

rocker-bogie suspension of a planetary rover, as shown in Figure 2. It plays a significant role in the manoeuvrability of the rover on rough terrains. It is either top-mounted or bottom-mounted with its pivot at the centre of the chassis. While traversing rough terrains, it ensures that the wheels of the rover maintain uniform contact with the ground, allowing the pressure to be evenly distributed and thereby preventing slip. When the rover encounters an obstacle, it ensures that all the wheels except for the one in contact with the obstacle remain grounded so that there is maximum grip. The centre of gravity affects the tilt capability of the suspension system[4]. The differential also aids in turning the rover smoothly by balancing the chassis roll and pitch angle. The differential rotates while achieving different speeds at equal torque on the pair of driving wheels[5]. It also absorbs the surface undulations, thereby acting as a shock absorber, which in turn stabilises the rover. Figure 1 shows all the parts of the rover assembly.

2.0 Force Analysis of Differential Bar

Figure 3 describes the geometry of the rover, including the suspension link lengths, ground clearance, wheel-to-wheel distance, and the angle subtended by the joints.

The following is the data considered for the analysis of the rover:

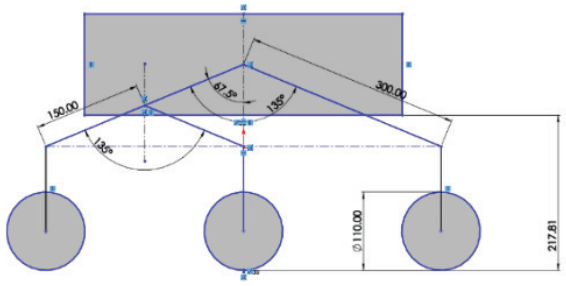


Figure 3. Rover geometry.

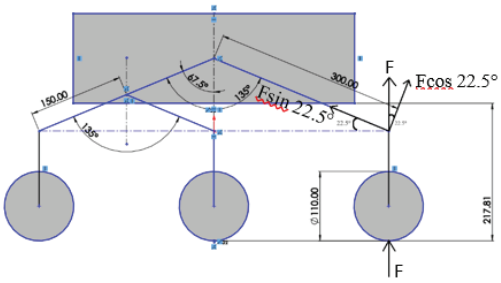


Figure 4. Free body diagram.

Weight of the Rover (W) = 15 kg = 150N

Lateral Distance from centre of the rover to each wheel (D) = 245mm = 0.245m

Length of the Rocker Arm (Lr) = 300mm = 0.3m

Length of the Bogie Arm (Lb) = 150mm = 0.15m

Wheel load (F) can be calculated by $= \frac{Rover\ weight}{Number\ of\ wheels} = \frac{150}{6} = 25N$

Force on Rocker Arm = Wheel Load = 25*N*

Now,

For calculating the Moment on the rocker arm, we need a force acting perpendicular to the rocker arm. Therefore, resolving the force acting on the rocker arm into 2 components, *i.e.*, 25*cos*22.5° and 25*sin*22.5° (Figure 4).

∴ Moment on the rocker arm (M_r) = 25*cos*22.5° × 0.3 = = 6.93 *Nm*

Distance between the rocker arms on either side of the chassis = 490mm = 0.49m

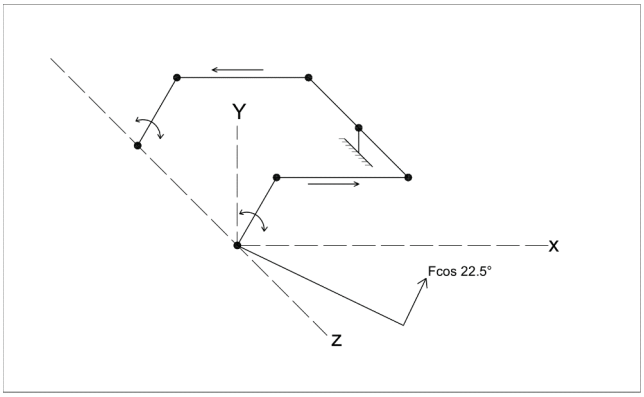


Figure 5. A diagrammatic representation of the direction of force acting on the differential bar.

Now,

$$\text{Force acting on the differential bar } (F_d) = \frac{\textit{Moment on the rocker arm}}{\textit{Distance between the rocker arm}/2}$$

$$= \frac{6.93}{0.49/2}$$

$$= 28.285N$$

Considering a safety factor of 1.5 due to variable loading conditions, uncertain environmental conditions and over time changes. FOS of 1.5 was considered as it keeps a balance between lightweight design and cost effectiveness.

$$\therefore \text{Force acting on the differential bar} = 28.285 \times 1.5$$

$$= 42.43N$$

$$\approx 43N$$

Figure 5 shows the directions of forces and moments acting on the links of the differential system.

3.0 Material Properties

The properties of materials used in the aerospace industry rely on the ability of the metal to withstand fracture upon impact and propagate cyclic cracks up to a certain limit. The materials having the required tensile strength, corrosion-resistant properties, and high mechanical strength do not necessarily mean that they are the ideal choices[6]. For the analysis, a set of suitable materials was selected considering the impact of various environmental conditions.

The materials are as follows:

- Aluminium 6061 T6
- Aluminium Alloy
- Ti-6Al-4V Titanium alloy
- Stainless steel 316 annealed
- Carbon Fibre 230 GPa

Aluminium 6061 T6 and aluminium alloy, due to their market availability, low cost, high strength-to-weight ratio, light weight, and flexible fabrication, aluminium alloys have become the mainstay of the aerospace industry[7]. Ti-6Al-4V titanium alloy is being widely used in aerospace industrial applications due to its high strength-to-weight ratio, corrosion resistance, ease of weldability and high temperature stability. Ti-6Al-4V possesses some excellent material characteristics which is inclined towards aiding in the manufacturability of critical aerospace components[8]. Stainless Steel is considered due to its corrosion-resistant properties, elevated temperature stability with high strength, ease of fabrication and can withstand high-pressure environments. Lastly, Carbon fibre gives a very high strength and durability as compared to its weight, and also it provides excellent structural integrity, which can be used in flexible designs[9]. Table 1 shows the properties of all these materials. Aluminium 6061 T6 consists of aluminium, chromium, copper, iron, magnesium, silicon and zinc[10]. Ti-6Al-4V consists of vanadium, aluminium, tin, zirconium, molybdenum, carbon, silicon, chromium, nickel, iron, copper, niobium and titanium[11]. Stainless Steel consists of carbon, manganese, silicon, chromium, nickel, molybdenum, phosphorus, sulphur, nitrogen and iron[12]. Carbon fibre comprises carbon, aluminium, silicon and oxygen[13].

4.0 Finite Element Analysis

Now, to calculate the maximum deformation, maximum stress and strain acting on the differential bar, static structural analysis was performed using ANSYS Workbench 2021[14] software.

The procedure followed for the analysis is:

- Firstly, the solid model of the differential bar designed on SolidWorks 2022[15], as shown in Figure 6, was imported into ANSYS Workbench.

Table 1. Summarized properties

Property	Aluminium 6061 T6	Aluminium alloy	Ti-6Al-4V titanium alloy	Stainless steel 316 annealed	Carbon fibre 230 GPa
Density (kg/m^3)	2713	2770	4429	7969	1800
Tensile Yield Strength (x10^8 Pa)	2.592	2.4	8.46	2.521	9
Tensile Ultimate Strength (x10^8 Pa)	3.131	3.1	9.18	5.651	-
Young's Modulus (GPa)	69	69	74	190	350

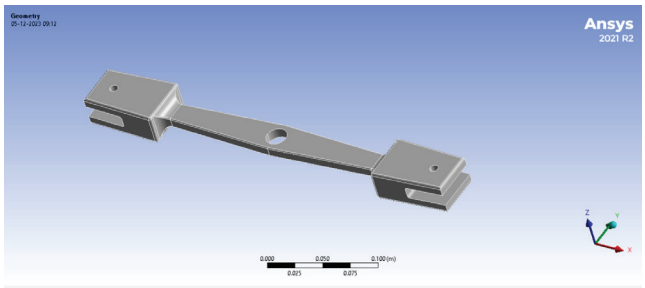


Figure 6. Solid model of differential bar.

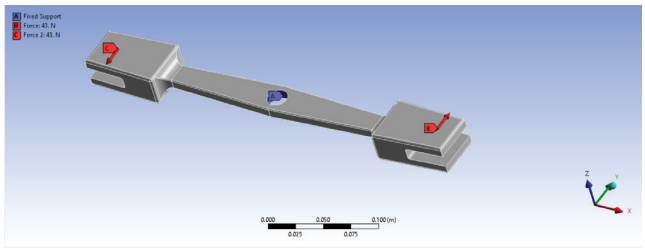


Figure 7. Meshing of the differential bar.

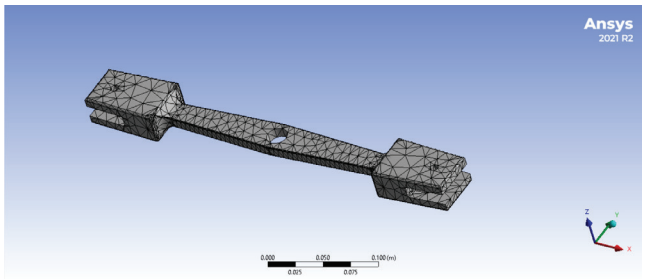


Figure 8. Boundary conditions.

- Required materials were selected from the material database. In the mechanical workspace, the material was applied to the model. A triangular element was chosen for meshing because the differential bar is a complex model and a triangular element is better for covering maximum of the area of the design without leaving gaps. Thereafter, meshing was performed using a triangular element with a mesh size of 0.01m. As the thickness is less compared to the length and width of the differential bar, therefore 2D element, *viz.* triangular element, was used for meshing.
- The required mesh was obtained as shown in Figure 7. Now, according to the analytical calculations and the integration of the differential bar onto the rover, boundary conditions were applied.
- Since the differential bar is to be pivoted at the centre of its geometry, it was top mounted onto the chassis and the centre of the bar was fixed, and the analytically calculated force of 43 N was applied onto the differential bar (Figure 8) which causes its swaying motion and the maximum stress, strain and deformation was analysed.

5.0 Results and Discussions

The analysis of the differential bar was done using 5 materials as follows:

1. Aluminium 6061 T6
2. Aluminium Alloy
3. Ti-6Al-4V Titanium alloy
4. Stainless steel 316 annealed
5. Carbon Fibre 230 GPa

5.1 FEA of Material 1- Aluminium 6061 T6

Figure 9 shows the amount of total deformation occurring when the load is applied; the blue area with the least deformation, and the red area being the maximum deformation, which accounts for 8.0133×10^{-5} m. Figure 10 shows the amount of Equivalent Elastic Strain occurring

when the load is applied; the blue area being the least strained and the red area being the most strained, which accounts for 9.0722×10^{-5}. Figure 11 shows the amount of Von-Mises Stress occurring when the load is applied; the blue area being the least stressed and the red area being the most stressed, which accounts for 6.2372×10^{6}. Figure 12 illustrates the variation in the graphs of total deformation, equivalent strain and stress.

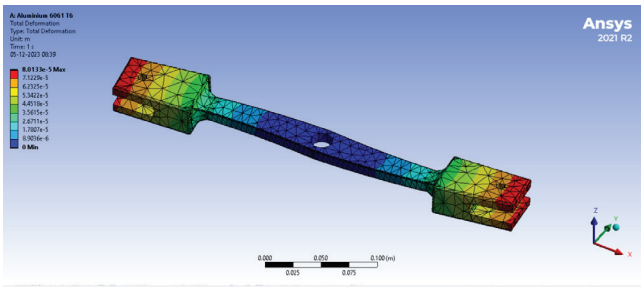


Figure 9. Total deformation of the differential bar.

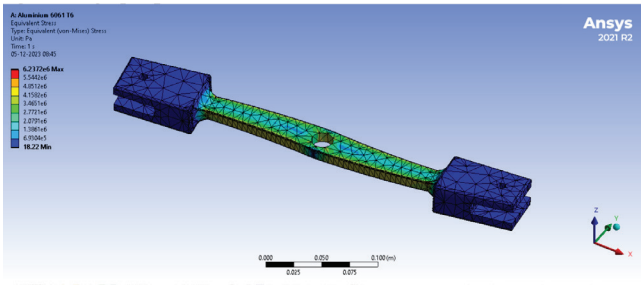


Figure 10. Equivalent (von-Mises) stress.

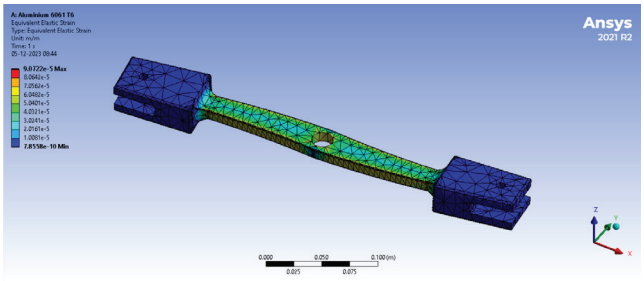


Figure 11. Equivalent elastic strain.

5.2 FEA of Material 2- Aluminium Alloy

Figure 13 shows the amount of total deformation occurring when the load is applied; the blue area with the least deformation, and the red area being the maximum deformation, which accounts for 7.7921×10^{-5} m. Figure 14 shows the amount of Equivalent Elastic Strain occurring when the load is applied; the blue area being the least strained and the red area being the most strained, which accounts for 8.8218×10^{-5}. Figure 15 shows the amount of Von-Mises Stress occurring when the load is applied; the blue area being the least stressed and the red area being the most stressed, which accounts for 6.2372×10^{6}. Figure 16 illustrates the variation in the graphs of total deformation, equivalent strain and stress.

5.3 FEA of Material 3- Ti-6Al-4V Titanium Alloy

Figure 17 shows the amount of total deformation occurring when the load is applied; the blue area with the least deformation, and the red area being the maximum deformation, which accounts for 4.978×10^{-5} m. Figure 18 shows the amount of Equivalent Elastic Strain occurring when the load is applied; the blue area being the least strained and the red area being the most strained, which accounts for 5.6186×10^{-5}. Figure 19 shows the amount of Von-Mises Stress occurring when the load is applied; the blue area being the least stressed and the red area being the most stressed, which accounts for 6.2219×10^{6}. Figure 20 illustrates the variation in the graphs of total deformation, equivalent strain and stress.

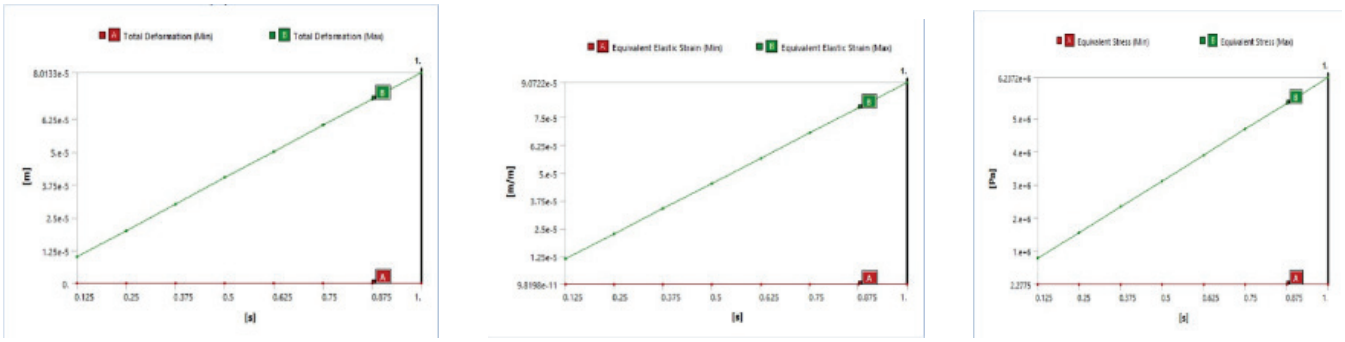


Figure 12. Graph of total deformation, equivalent strain and stress.

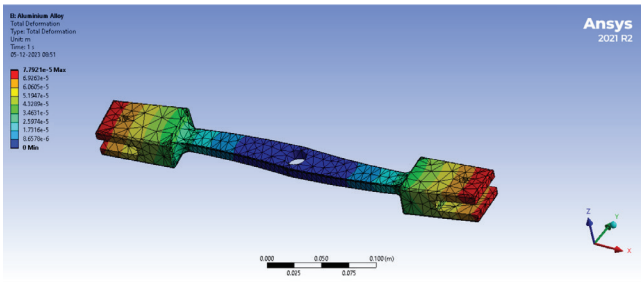


Figure 13. Total Deformation of the differential bar.

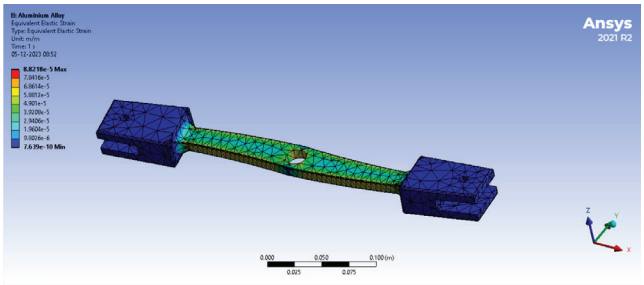


Figure 14. Equivalent elastic strain.

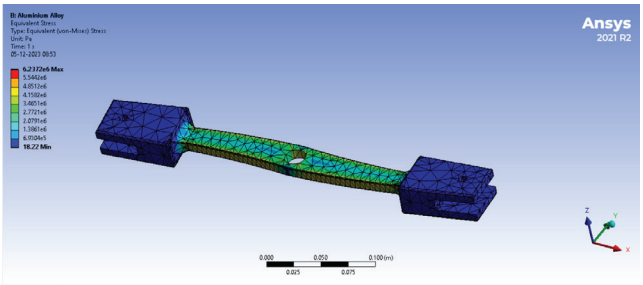


Figure 15. Equivalent (von-Mises) stress.

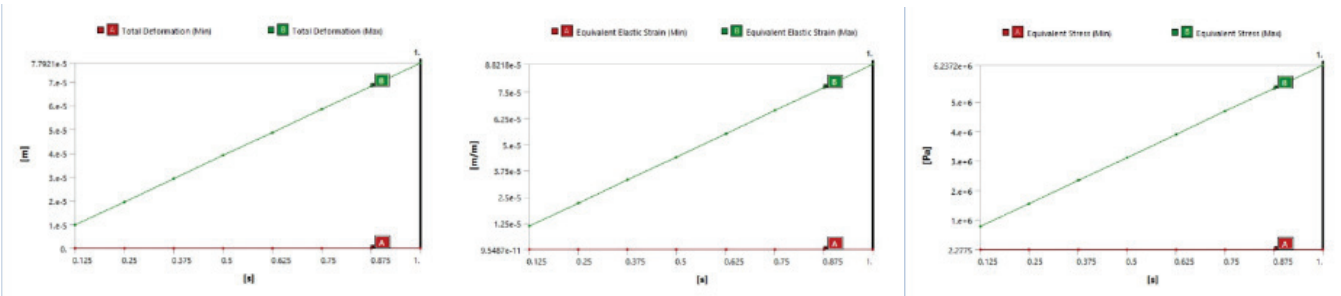


Figure 16. Graph of total deformation, equivalent strain and stress.

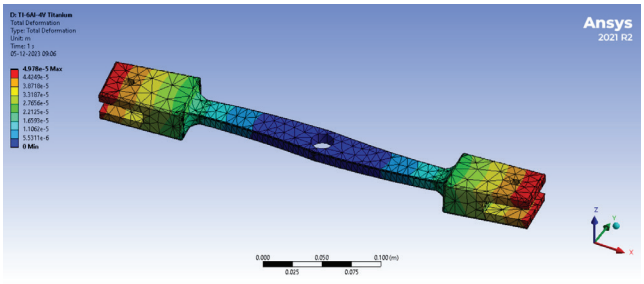


Figure 17. Total deformation of the differential bar.

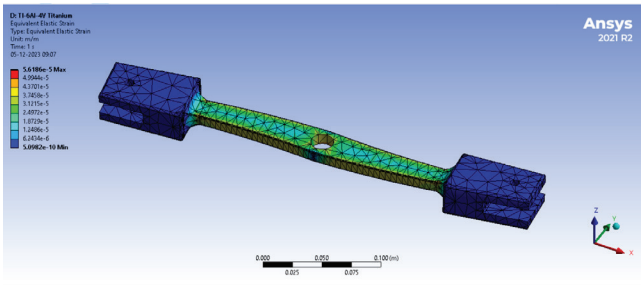


Figure 18. Equivalent elastic strain.

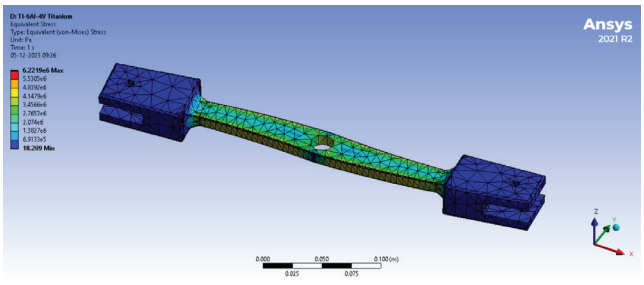


Figure 19. Equivalent (von-Mises) stress.

5.4 FEA of Material 4- Stainless Steel 316 Annealed

Figure 21 shows the amount of total deformation occurring when the load is applied; the blue area with the least deformation, and the red area being the maximum deformation, which accounts for 2.8253×10^{-5} m. Figure 22 shows the amount of Equivalent Elastic Strain occurring when the load is applied; the blue area being the least strained and the red area being the most strained, which accounts for 3.2625×10^{-5}. Figure 23 shows the amount of Von-Mises Stress occurring when the load is applied;

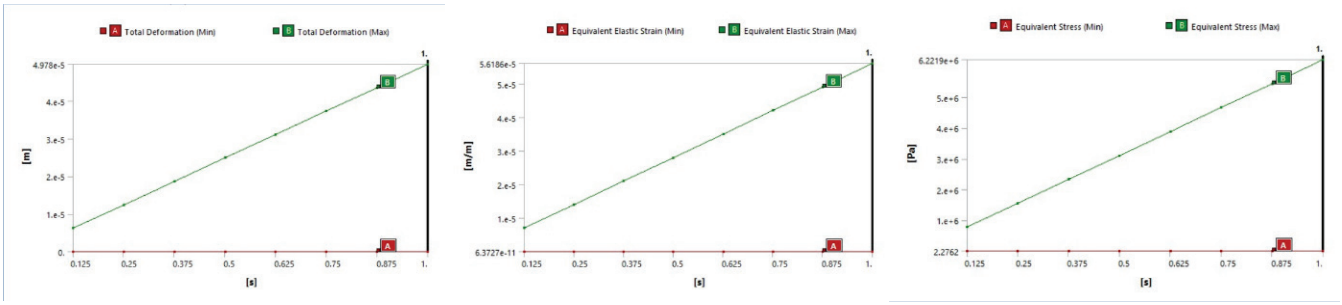


Figure 20. Graph of total deformation, equivalent strain and stress.

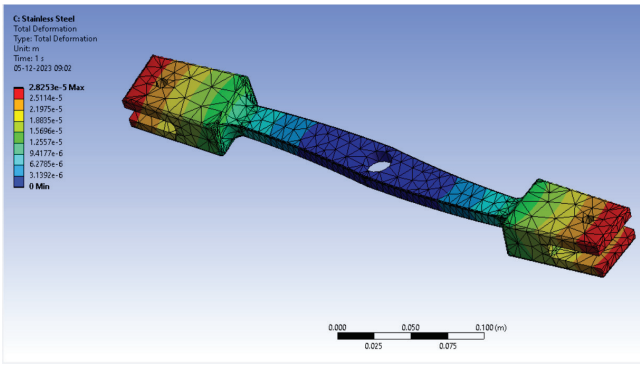


Figure 21. Total deformation of differential bar.

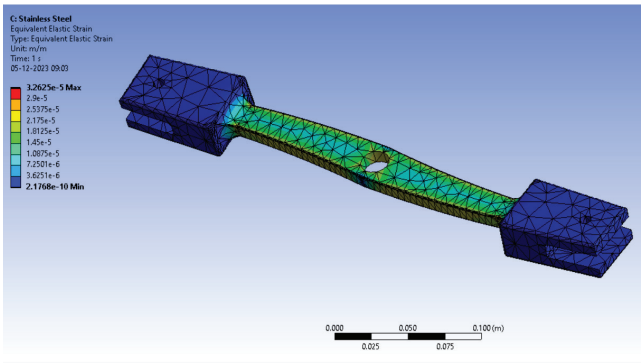


Figure 22. Equivalent elastic strain.

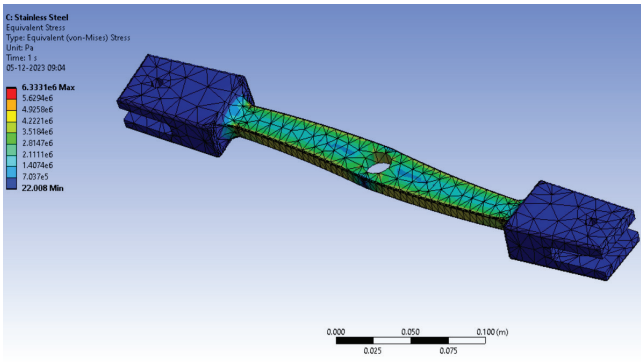


Figure 22. Equivalent (von-Mises) stress.

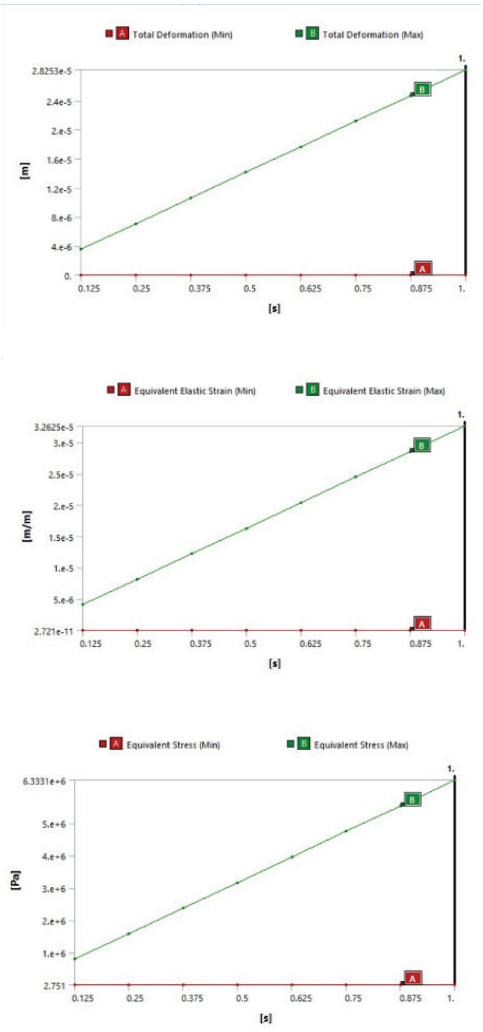


Figure 24. Graph of total deformation, equivalent strain and stress.

the blue area being the least stressed and the red area being the most stressed, which accounts for 6.3331×10^6. Figure 24 illustrates the variation in the graphs of total deformation, equivalent strain and stress.

5.5 FEA of Material 5- Carbon Fibre 230 GPa

Figure 25 shows the amount of total deformation occurring when the load is applied; the blue area with the least deformation, and the red area being the maximum deformation, which accounts for 4.2029×10^{-5} m. Figure 26 shows the amount of Equivalent Elastic Strain occurring when the load is applied; the blue area being the least strained and the red area being the most strained, which accounts for 0.00017436. Figure 27 shows the amount of Von-Mises Stress occurring when the load is applied; the blue area being the least stressed and the red area being the most stressed, which accounts for 1.3545×10^{7}. Figure 28 illustrates the variation in the graphs of total deformation, equivalent strain and stress. Table 2 shows a comparison of maximum stress (Pa), Maximum Deformation (m) and Maximum Strain for the various materials analysed for the differential bar.

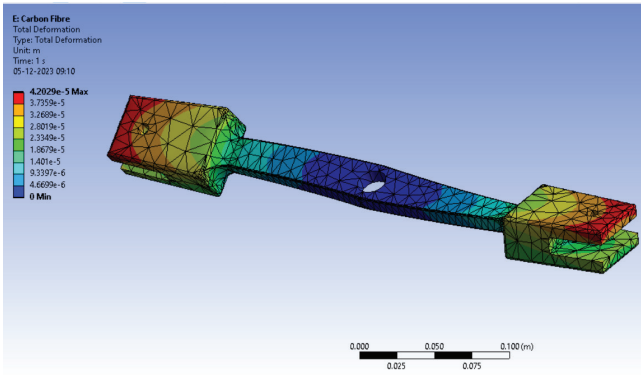


Figure 25. **Total deformation of differential bar.**

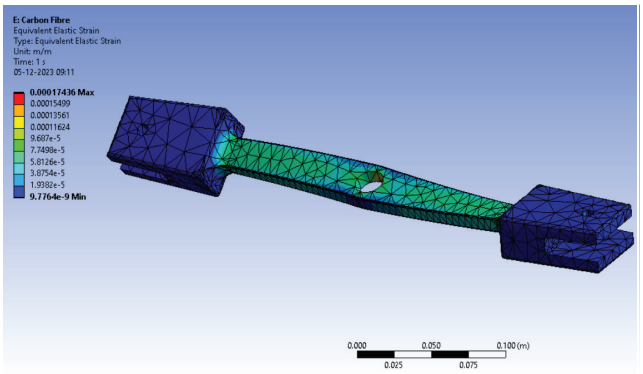


Figure 26. **Equivalent elastic strain.**

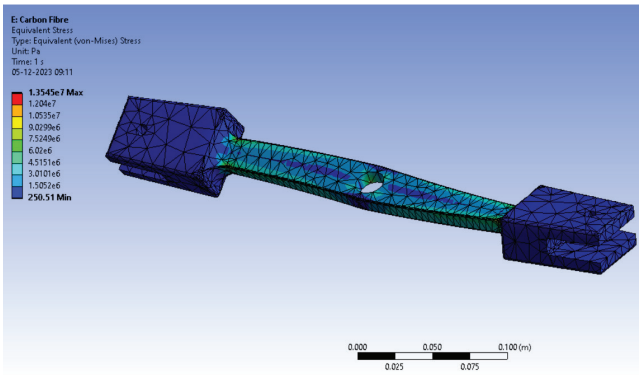


Figure 27. **Equivalent (von-Mises) stress.**

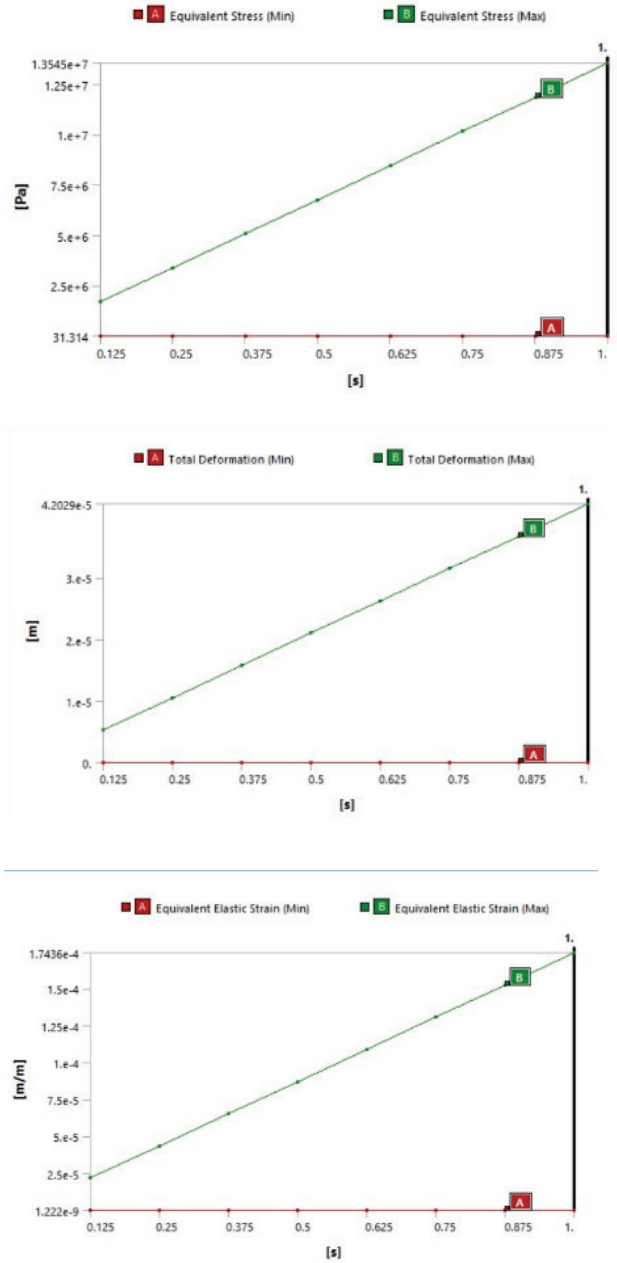


Figure 28. Graph of total deformation, equivalent strain and stress.

Table 2. Summarised results

S. No.	Material	Maximum stress (Pa)	Maximum deformation (m)	Maximum strain
1	Aluminium 6061 T6	$6.237x10^{6}$	$8.013x10^{-5}$	$9.072\ x10^{-5}$
2	Aluminium alloy	$6.237x10^{6}$	$7.792x10^{-5}$	$8.822\ x10^{-5}$
3	Ti-6Al-4V titanium alloy	$6.232x10^{6}$	$4.978\ x10^{-5}$	$5.619\ x10^{-5}$
4	Stainless steel 316 annealed	$6.333x10^{6}$	$2.825x10^{-5}$	$3.263\ x10^{-5}$
5	Carbon Fibre 230 GPa	$1.355x10^{7}$	$4.203x10^{-5}$	$1.744\ x10^{-4}$

6.0 Conclusion

In this paper, Finite Element Analysis (FEA) of a differential bar has been performed for the five materials. From the FEA results, it was observed that the maximum stress induced in the considered materials is almost the same, except for the Carbon Fibre material. Considering the deformation, the least value obtained was 2.825×10^{-5} m for the Stainless steel 316 annealed material. The next significant least value of maximum deformation was observed at Carbon Fibre 230 GPa, *i.e.*, 4.203×10^{-5} m, followed by Ti-6Al-4V Titanium alloy, Aluminium Alloy and Aluminium 6061 T6 with a deformation of 4.978×10^{-5} m, 7.792×10^{-5} m and 8.013×10^{-5} m, respectively. Now, while selecting the most optimum material, Aluminium 6061 T6 was ruled out because it was not good enough to withstand impact forces. Though Aluminium alloy is light in weight and has a good strength-to-weight ratio, it cannot withstand extreme environmental conditions like temperature variations and vacuum in space. Carbon Fibre material was eliminated due to its complexity in manufacturing and cost concerns. The exposure of Carbon Fibre to vacuum environments releases certain gases, which can contaminate the sensitive instruments. Now, Stainless Steel and Ti-6Al-4V Titanium alloy were compared on the basis of weight criteria, as it is one of the critical factors that influences their overall performance. Titanium outperforms Stainless Steel, *i.e.*, the differential bar weighs 0.999kg when made from titanium, which increases to 1.7979 kg in the case of Stainless Steel. This is because titanium has a lower density as compared to stainless steel and is being widely used in aerospace applications. Therefore, the appropriate material chosen for the differential bar is Ti-6Al-4V Titanium alloy. The design of the differential bar of this type is limited to 6-wheeled rocker bogie type rovers only. The analysis was performed using FEA; the validation of FEA results with either analytical or experimental results could be a future recommendation for this work.

7.0 References

1. Woodall M, Baechler G, Salehinia I, Pohlman N. A. Mars rover Rocker-Bogie comparative differential study. ResearchGate. 2020; 9(4).
2. Jordan E. Mars science laboratory differential restraint: The devil is in the details. NASA Technical Reports Server (NTRS); 2012.
3. Manik MD, Chauhan AS, Chakraborty S, Tiwari VR. Experimental analysis of climbing stairs with the Rocker-Bogie mechanism. Int J Adv Res Innov Ideas Educ. 2016; 2(2):957-960.
4. Chinchkar DS, Gajghate SS, Panchal R, Shetenawar RM, Mulik P. Design of Rocker Bogie mechanism. Int Adv Res J Sci Eng Technol. 2017; 2(5):312-338.
5. The Mechanic. Differential (mechanical device).
6. Sanderson L. Stainless steels and alloys in air and space-craft. Aircr Eng Aerosp Tech. 1976; 48(12):24-27. https://doi.org/10.1108/eb035361
7. El-Hameed AMA, Abdel-Aziz YA. Aluminium alloys in space applications: A short report. J Adv Res Appl Sci Eng. Technol. 2021; 22(1):1-7. https://doi.org/10.37934/araset.22.1.17
8. Gomez-Gallegos A, Mandal P, Gonzalez D, Zuelli N, Blackwell P. Studies on titanium alloys for aerospace application. Defect Diffus. Forum. 2018; 385:419-423. https://doi.org/10.4028/www.scientific.net/DDF.385.419
9. Guo QF, Li W, Dong JH, Li YC, Wang KJ, Wang HP, *et al.* Application of carbon fiber composite on space camera frame. Adv Mater Res. 2011; 194-196:1558-1563. https://doi.org/10.4028/www.scientific.net/AMR.194-196.1558
10. Kang SW, Jang BS. Friction stir welding analysis based on equivalent strain method using neural networks. J Ocean Eng Technol. 2014; 28(5):452-465. https://doi.org/10.5574/KSOE.2014.28.5.452
11. Polishetty A, Littlefair G, Kumar KP. Machinability assessment of titanium alloy Ti-6Al-4V for biomedical applications. Adv Mat Res. 2014; 941-944:1985-1990. https://doi.org/10.4028/www.scientific.net/AMR.941-944.1985
12. Bukuaghangin O, Sanni O, Neville A, Charpentier T. A kinetic study of barium sulphate formation in presence of scale inhibitor in a flowing system. Corrosion. 2016; 1-14. https://doi.org/10.5006/C2016-07635
13. Orbulov I, Németh Á, Dobranszky J. XRD and EDS investigations of metal matrix composites and syntactic foams; 2008. p. 1-10.
14. ANSYS Workbench 2021 R2, ANSYS Inc.; 1970
15. SolidWorks 2022. Dassault Systems.